Langmuir

Article

pubs.acs.org/Langmuir

Microstructure, Morphology, and Ultrafast Dynamics of a Novel Edible Microemulsion

Ranajay Saha, Surajit Rakshit, Rajib Kumar Mitra,* and Samir Kumar Pal*

Department of Chemical, Biological & Macromolecular Sciences, S.N. Bose National Centre for Basic Sciences, Block JD, Sector III, Salt Lake, Kolkata 700098, India

Supporting Information

ABSTRACT: An edible microemulsion (ME) composed of Tween 80/butyl lactate/isopropyl myristate (IPM)/water has been formulated. Pseudoternary phase diagram of the system contains a large single isotropic region. The phase behavior of the system is also studied at low pH (2.6) and in 0.9% NaCl solution. Conductivity, viscosity, ultrasonic velocity, and compressibility studies find consistent results in the structural transition (from water-in-oil (w/o) to bicontinuous, and from bicontinuous to oil-in-water (o/w)) behavior of the ME. Dynamic light scattering studies reveal the size of the MEs. The absorption and steady state emission spectra of 4-(dicyanomethylene)-2-methyl-6-(p-dimethylamino-styryl)-4H-pyran (DCM) successfully probe the polarity of the ME at its solvation shell and shows the efficacy of hosting model drug molecules. The rotational anisotropy of the dye has been studied to ascertain the geometrical restriction of the probe molecule. Picosecond-resolved fluorescence spectroscopy applies well to study the relaxation dynamics of water in the solvation shell of the MEs. The study finds strong correlation in the relaxation dynamics of water with the structure of host assembly and offers an edible ME system which could act as a potential drug delivery system and nontoxic nanotemplate for other applications.

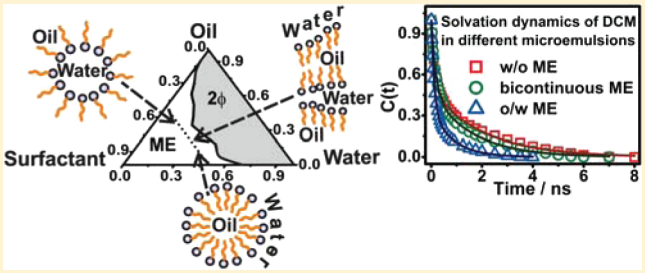

INTRODUCTION

The design and development of new drug delivery systems with a view to enhancing the efficacy of existing drugs is an ongoing process in pharmaceutical research. Recently, a great deal of dosage form development activity has focused on the employment of microemulsions (MEs) as drug delivery systems. MEs are considered ideal for drug delivery due to their thermodynamic stability (i.e., a long shelf life), low viscosity, ease of preparation, improved drug stability and solubility, surfactant-provoked permeability, and protection against enzymatic degradation.[1] Owing to the nanometric size, MEs improve transdermal diffusivity of drugs in cutaneous application.[2] However, the limitations on the use of MEs in pharmaceutical and cosmetic fields arise greatly from the need for all the constituting components to be biologically and pharmaceutically acceptable, particularly the surfactant and cosurfactant. Most of the work found in the literature[3−5] has been related to the use of either ionic surfactants or nonionic surfactants that require the presence of short chain alcohol or amine cosurfactants to form MEs. In general, medium chain alcohols are found to be the most efficient promoters for ME formulation.[6] However, synthetic surfactants and short or medium chain alkanols as cosurfactants produce potential skin irritation or allergy.[7,8] On top of that, destabilization of the system by evaporation of volatile alcohols prevent these ME formulations from being used for practical applications.[9] Therefore, the selection of components for MEs suitable for cosmetic and pharmaceutical use is one of the most important factors to fulfill the requirements of a good delivery system. Several attempts have been carried out to substitute alkanols by other ingredients such as amines,[3,10] nonionic surfactants,[11] and glycolic derivatives;[12] however, the use of the well-known pharmaceutical flavoring agent butyl lactate[13] as a cosurfactant in ME formation is less known[14] and could stand up as a good replacement of the contemporary cosurfactants. Butyl lactate is obtained from renewable resources and is considered as a safe[15] and biodegradable product with an oral LD_{50} value greater than 2000 mg/kg[15] for a rat. As such, butyl lactate is a permitted food additive for human consumption.[16] It could be argued that hydrolysis of butyl lactate in the low pH region like the stomach can release *n*-butanol, which could appear as a major concern with regard to its stability as well as its edibility. However, the solubility of butyl lactate in water is very low (4.2%, v/v)[17] and hence the produced *n*-butanol will be present only in a trace amount, as the reaction has a fairly low rate constant of 8.7×10^{-3} L $mol^{-1}min^{-1}$ at 30 ^{o}C.[18] More importantly, the acute toxicity of *n*-butanol is fairly low, with an oral LD_{50} value of 790−4360 mg/kg for a rat.[19,20] In fact, the human body has a known pathway to metabolize *n*-butanol in a manner similar to ethanol: alcohol dehydrogenase coverts *n*-butanol to butyraldehyde; this is then converted to butyric acid by aldehyde dehydrogenase. Butyric acid can then be fully metabolized to carbon dioxide and water by the β-oxidation

Received: January 2, 2012
Published: May 9, 2012

   dx.doi.org/10.1021/la3012124 | *Langmuir* 2012, 28, 8309−8317

pathway.[15] The use of butyl lactate as a cosurfactant to substitute pentanol has earlier been shown to increase the solubilization capacity of ME.[14] In the present contribution, we use butyl lactate as a cosurfactant in the formulation of a Tween-based ME and characterize the internal structure of the ME, which is necessary for its pharmaceutical application concerning drug solubility, stability, and its release.

The structure of ME can be idealized as a set of interfaces dividing polar and nonpolar domains. Depending on the composition of the system, the microstructure of an ME may exist as water-in-oil (w/o) droplets, oil-in-water (o/w) droplets, or a bicontinuous structure. Various spectroscopic techniques such as small-angle X-ray scattering (SAXS), dynamic light scattering (DLS), pulsed-gradient spin−echo (PGSE) nuclear magnetic resonance spectroscopy, and others have been employed for structural identification of these systems.[21−24] Moreover, there is a growing interest to study the behavior of water molecules in such organized assemblies. Interestingly, water molecules confined in organized assemblies (reverse micelles, micelles, vesicles) and various biological macromolecules (such as protein surfaces or DNA) strongly influence the structure, function, and dynamics of biomolecules.[25] Pharmaceuticals have displayed enhanced structural and conformational stability and slow diffusivity,[26] and certain enzymes manifest enhanced activity at certain levels of hydration[26] in the ME system. Garti and co-workers have employed the subzero DSC technique to study the nature of the water and its thermal behavior in ME systems.[27] Water confined in reverse micelles has been detailed by Amararene et al. using acoustic and densimetric experiments.[28] NMR studies have successively reported the diffusive property of water in these types of nonoconfining environments. With this background, the dynamics of water in such nanocavity seems interesting and can be studied using various techniques such as solvation dynamics.

In the present study, an attempt has been made to construct an ME system comprising the pharmaceutically acceptable components Tween 80/butyl lactate/isopropyl myristate (IPM)/water.[13,29,30] A pseudoternary phase diagram has been constructed for the chosen system at a constant surfactant/cosurfactant weight ratio of 1:1. Conductivity, viscosity, ultrasonic compressibility, and sound velocity measurements are employed to investigate the gradual changes occurring in the microstructure of the MEs with increasing water content. The bound property of water at the surfactant water interface has successfully been studied by the solvation probe 4-(dicyanomethylene)-2-methyl-6-(p-dimethylamino-styryl)-4H-pyran (DCM) using the picosecond time-resolved fluorescence spectroscopy technique. To ascertain the geometrical restriction of the probe at the interface, rotational relaxation dynamics of the dye in different ME systems have also been determined. In relation to the microenvironment polarity, the steady state absorption and emission data of DCM at the interface has been monitored as a function of water concentration. The focus of this paper is the formulation and physicochemical characterization of the ME formed using pharmaceutically acceptable components in a wide composition range in order to obtain information on self-organized structures. The study focuses to find correlation in the water relaxation dynamics with the structure of the host assembly. It is believed that the findings would show the convenience of characterizing ME systems from a physicochemical and spectroscopic point of view and improve our understanding of the microstructure of such ME systems. This will serve as a basis for further investigations of ME systems useful in drug delivery and as nontoxic nanotemplates for other applications.

MATERIALS AND METHOD

Chemicals were obtained from the following sources: DCM (Fluka); IPM (Sigma Aldrich); butyl lactate (Spectrochem); polyoxyethylene-sorbitan monooleate (Tween 80, Sigma Aldrich); sodium chloride (Merck); *n*-butanol (SRL); sodium citrate (Aldrich); citric acid (Merck). All samples were of highest commercially available purity and used without further purification. Double distilled water was used throughout the experiments. The pseudoternary phase diagrams were constructed to investigate the concentration ranges of components for identifying the existence of ME regions by the water titration method, using oil (IPM), surfactant (Tween 80), cosurfactant (butyl lactate), and double distilled water at room temperature with a constant surfactant/cosurfactant weight ratio (1:1). IPM was mixed with Tween 80/butyl lactate mixture; water was then added dropwise (10 μL) using a micropipet until the transparent and homogeneous dispersion converted to turbid mixture. The appearance of turbidity was considered as an indication of phase separation. The ME regions were identified as optically transparent and isotropic mixtures. Pseudoternary phase diagrams of the system were also constructed at acidic pH (sodium citrate buffer, pH 2.6) and 0.9% NaCl solution.

The electrical conductivity of the ME was measured using a Sension378 conductivity meter (Hach Company, Loveland, CO) at room temperature. Conductivity measurements were carried out by titration of oil and the surfactant/cosurfactant mixture with water

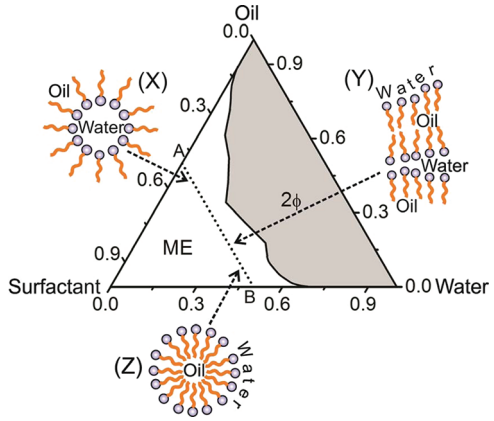

Figure 1. Pseudoternary phase diagram of the Tween 80/butyl lactate/IPM/water ME system. (2Φ) Two-phase region, (ME) single-phase region, (X) w/o ME, (Y) bicontinuous ME, (Z) o/w ME. The dotted line AB represents the dilution line along which all the experiments are carried out.

(along the dilution line AB, in Figure 1). Since the MEs were based on nonionic components and there is no considerable dependence of phase behavior on salinity, a solution of 0.9% NaCl was used as the titrant in place of pure water. Measurement of conductivity was carried out with an absolute accuracy up to ±0.5%.

Compressibility of the mixtures were calculated using the density and sound velocity values measured by a density meter (model DSA5000) from Anton Paar (Austria) with an accuracy of 5×10^{-6} g cc^{-1} and 0.5 ms^{-1} in density and sound velocity measurements, respectively. Adiabatic compressibility (β) of the MEs can be determined by solution density (ρ) and the sound velocity (u) and applying Laplace's equation,

$$\beta = \frac{1}{\rho \times u^2} \quad (1)$$

dx.doi.org/10.1021/la3012124 | *Langmuir* 2012, 28, 8309−8317

Viscosities of MEs were obtained along the dilution line AB (Figure 1) by measuring the flow times in a calibrated Ostwald viscometer having 100 s efflux time for water. Densities of MEs measured was used for viscosity calculation using the following equation:

$$\eta = \eta_w \frac{t \times \rho}{t_w \times \rho_w} \quad (2)$$

where η denotes viscosity, ρ is density, and t is the time of flow of the respective systems.

The hydrodynamic diameter of ME nanodroplets was determined using the DLS instrument from Nano S Malvern employing a 4 mW He−Ne laser (λ= 632.8 nm) equipped with a thermostatted sample chamber. All the scattered photons were collected at a 173° scattering angle. The scattering intensity data were processed using the instrumental software to obtain the hydrodynamic diameter (d_H) and the size distribution of the scatterer in each sample. The instrument measures the time-dependent fluctuation in the intensity of light scattered from the particles in solution at a fixed scattering angle. The hydrodynamic diameter (d_H) of the nanodroplet is estimated from the intensity autocorrelation function of the time-dependent fluctuation in intensity. d_H is defined as

$$d_H = \frac{k_B T}{3\pi\eta D} \quad (3)$$

where k_B is the Boltzmann constant, η is the viscosity, D is the translational diffusion coefficient, and T is the temperature. The viscosity of the ME determined was used as the viscosity of the dispersant. DLS experiments were done in triplicate with at least 15 runs per measurement.

Steady-state emission spectra were measured with a Jobin Yvon Fluoromax-3 fluorimeter. Fluorescence transients were measured using commercially available spectrophotometer (LifeSpec-ps) from Edinburgh Instrument, U.K. (excitation wavelength 409 nm, 80 ps instrument response function (IRF)) and fitted using F900 software provided by Edinburgh Instrument. Briefly, the observed fluorescence decay transients were fitted by using a nonlinear least-squares fitting procedure to a function ($X(t) = \int_0^t E(t')R(t - t')dt'$) comprising convolution of the IRF ($E(t)$) with a sum of exponentials ($R(t) = A + \sum_{i=1}^{N} B_i e^{-t/\tau_i}$) with pre-exponential factors (B_i), characteristic lifetimes (τ_i) and a background (A). Relative concentration in a multi-exponential decay is finally expressed as $a_n = B_n/\sum_{i=1}^{N} B_i$. The quality of the curve fitting is evaluated by reduced χ^2 and residual data.

To construct time-resolved emission spectra (TRES), we follow the technique described in refs 31 and 32. The time-dependent fluorescence Stokes shifts, as estimated from TRES, are used to construct the normalized spectral shift correlation function or the solvent correlation function, $C(t)$, defined as

$$C(t) = \frac{\nu(t) - \nu(\infty)}{\nu(0) - \nu(\infty)} \quad (4)$$

where $\nu(0)$, $\nu(t)$ and $\nu(\infty)$ are the emission maxima (in cm^{-1}) at time zero, t, and infinity, respectively. The $C(t)$ function represents the temporal response of the solvent relaxation process, as occurs around the probe following its photo excitation and the associated change in the dipole moment. For anisotropy ($r(t)$) measurements, emission polarization was adjusted to be parallel or perpendicular to that of the excitation, and anisotropy is defined as[31]

$$r(t) = \frac{I_{para}(t) - G \times I_{per}(t)}{I_{para}(t) + 2 \times G \times I_{per}(t)} \quad (5)$$

where $I_{para}(t)$ and $I_{per}(t)$ are the temporal emission intensities at parallel and perpendicular emission polarization with respect to vertical excitation polarization. G, the grating factor, was determined following the longtime tail matching technique.[31]

RESULTS AND DISCUSSIONS

Figure 1 shows the pseudoternary phase diagram of the system composed of Tween 80/butyl lactate/IPM/water at room temperature. The phase behavior, as shown in Figure 1, manifests a large single phase isotropic ME region, formed spontaneously at room temperature coupled with a two-phase region appearing along the oil−water axis. The isotropic mixtures of ME remain stable without any phase separation upon prolonged standing. For potential pharmaceutical application, the ME system should be stable at various physiologically relevant environments, and to check that, we observe the phase behavior at pH = 2.6 and also in 0.9% salt concentration. It is found that the phase behavior of the system remains almost unaltered at pH 2.6 (Figure 2a) as well as in

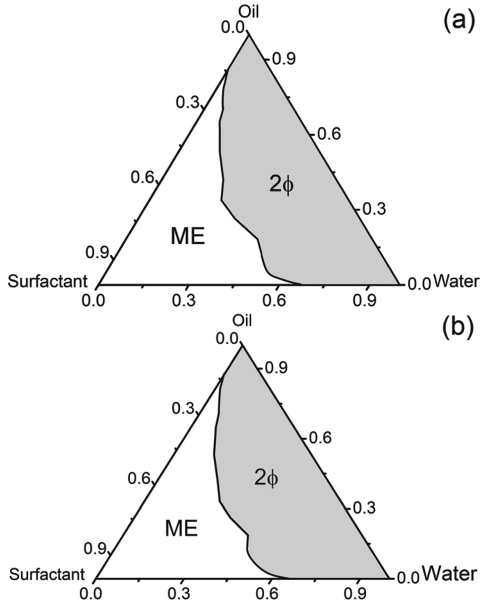

Figure 2. Pseudoternary phase diagram of Tween 80/butyl lactate/IPM/water ME system (a) at pH 2.6 and (b) at 0.9% NaCl. (2Φ) Two-phase region, (ME) single-phase region.

0.9% salt concentration (Figure 2b) revealing the stability of the system in such environments. As discussed earlier considering a finite possibility of butyl lactate being hydrolyzed to form *n*-butanol at in vivo low pH of the stomach, which may in turn affect the stability of the ME system, we construct the phase behavior of the system at various pH using *n*-butanol as the cosurfactant (Figures S1 and S2). As evidenced from the figures, only marginal change in the phase behavior is observed when butyl lactate is replaced by *n*-butanol. This firmly affirms that possible formation of *n*-butanol hardly affects the stability of the ME. This study further adds up to the potentiality of the ME system in pharmaceutical applications. Notably, line AB in Figure 1 shows the experimental path along which the measurement of physical properties is carried out. Line AB corresponds to a fixed surfactant/cosurfactant weight ratio of 1, with the weight fraction each in the total system being 0.25. The weight fraction of water (denoted by X_w) and oil varies through line AB.

It is well-known that in nonionic MEs at low water contents, discrete reverse micelles (w/o) are formed within a continuous oil phase, and the system shows electrical conductivity (σ) similar to that of the oil phase.[33,34] Conversely, systems with

dx.doi.org/10.1021/la3012124 | Langmuir 2012, 28, 8309−8317

high water content, forming normal micelles (o/w) within a continuous aqueous phase, show σ similar to that of pure water.[33,35] We measure σ as a function of X_w to identify the microstructure type of the ME phase in the present investigation. Figure 3a is a representative σ versus X_w profile

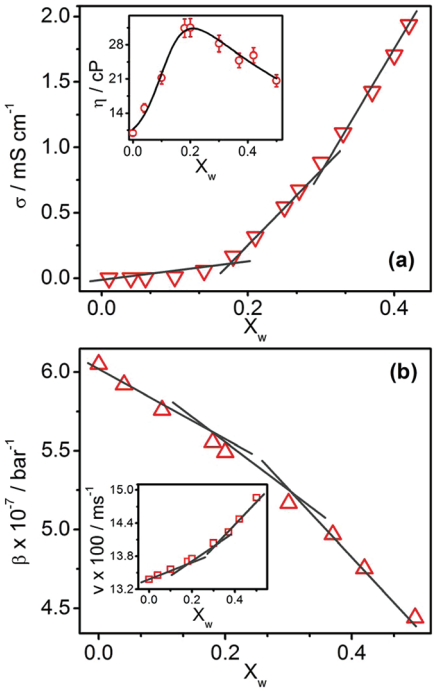

Figure 3. (a) Variation of electrical conductivity (σ) along the dilution line AB (X_w = wt. fraction of water); the inset shows the respective variation in viscosity (η). (b) Variation of ultrasonic compressibility (β) along the dilution line AB (X_w = wt. fraction of water); the inset shows the respective variation in ultrasonic velocity (v).

for the studied ME system along the dilution line AB of Figure 1. The curve can be divided into three distinct segments. In the oil-rich region, σ is very low and increases marginally with X_w. The poor conductivity of the system in this region is due to the closed domains of water present in w/o MEs. The low conductive oil continuous phase in this region prevents continuous migration of the charge carriers and hence explains the low conductivity of the water droplets (w/o). On further addition of water, σ increases and two sharp transition points are obtained at X_w = 0.18 and 0.30. The transition at X_w = 0.18 could be correlated with the formation of bicontinuous ME where various interconnected surfactant domains form a network of conductive channel allowing effective transport of charge carriers, and relatively higher values of σ can be realized.[36] The change in the slope of σ beyond X_w = 0.30 can be interpreted as a structural transition to o/w droplets. This transition takes place, as at high X_w the aqueous phase becomes the continuous phase with surfactant-coated oil droplets dispersed in it, and a significant connectivity between aqueous domains is established.

The structural transition in ME essentially involves droplet association, i.e., clustering and fusion. It must, therefore, have a direct influence on the internal structure and hence viscosity. Figure 3a (inset) shows the dynamic viscosity of the ME system along the dilution line AB. A bell-shaped viscosity profile with flattened maxima is obtained, as has earlier been reported using nonionic surfactants, Tween 60/ethanol/R(+)-limonene/water/propylene glycol,[37] and brij-35/butanol/eucalyptus oil/water.[38] The low initial viscosity of the system is attributed to the negligible interactions between the isolated "hard sphere-like" water globules dispersed in the continuous oil medium.[39] With gradual addition of water, dispersed water droplets grow, and the enhanced attractive interaction between them leads to the formation of water clusters. The increase in the viscosity in oil-rich MEs is thus derived from an increase in the dispersed droplet sizes and the enhanced attractive interactions between the droplets.[40] At the threshold composition, such clustering leads to the formation of a bicontinuous structure wherein the infinite radius of curvature of the aggregate results in the maximum viscosity of the system. In our study, the maximum of viscosity occurs at X_w = 0.20, wherein a bicontinuous ME is realized. Further addition of water causes a decrease in viscosity, indicating that water, which is the least viscous component of the ME system, becomes the outer phase, eventually forming o/w MEs. In this aqueous-rich region, viscosity gradually decreases expectedly due to dilution effect of the o/w ME droplets. The viscosity data thus corroborates with the conductivity data and specify that, with increasing water, the oil-continuous ME transforms into a bicontinuous form at X_w = 0.20 and with further addition of water ultimately transforms into the water continuous structure.

Ultrasonic velocity (v) in the ME system as a function of X_w is displayed in Figure 3b, inset. The value of v increases with the addition of water with small changes in the slope at two X_w values of ~0.18 and 0.30, suggesting structural evolution at these concentrations. We also measure isentropic compressibility β for all these systems, and the results are shown in Figure 3b. A consistent decrease of β is observed with increasing water content with sharp changes in slope identified at X_w values of about 0.18 and 0.30. The decrease in β with increasing X_w is expected, as the system becomes more water-like with increasing X_w. The higher compressibility of the system at low water content is in good agreement with the viscosity behavior of the system, which suggests the hard sphere-like character of the water globules in oil continuous medium (w/o).[39] The observed experimental trend of β with distinct changes in the slope suggests the deviation of elastic properties of water in the ME system, correlating the different structural identity of the ME. Such finding is well in agreement with the conductivity and viscosity behavior of the system, with structural transition at ~0.18 and 0.30 weight fraction of water.

Size characterization of the resulting ME is also essential in ensuring safe and efficient dosage. Monitoring of changes in the size distribution can provide valuable information for optimizing the formulation. Figure 4, inset, shows a typical DLS curve for the ME system along the dilution line AB with X_w being 0.42. The curve is single modal, and the peak is rather narrow, indicating the low polydispersity of the sample. Figure 4 summarizes the effect of sample composition on the droplet size of MEs. In general, the droplet size is small, ranging from 4.7 to 10.3 nm. This is in line with previously published data.[41,42] For w/o ME, the "lipodynamic" diameter increases expectedly with increasing water content, indicating larger size of the water pool at higher X_w.[42] However, for o/w MEs, the droplet size remains fairly constant with added water confirming their formation in the studied range of X_w. Notably the uncertain shape distribution of bicontinuous MEs prevents one from measuring its size by DLS, which assumes the aggregate shape is circular in size measurement.

dx.doi.org/10.1021/la3012124 | Langmuir 2012, 28, 8309−8317

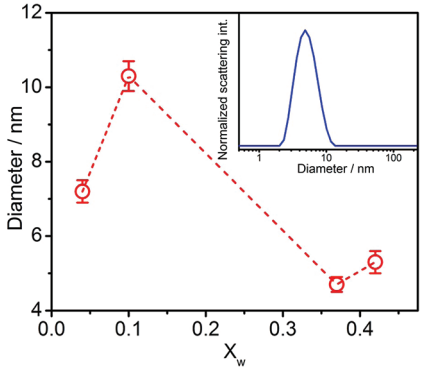

Figure 4. Diameter of MEs at various X_w values (X_w = wt. fraction of water). The dotted line is guide to the eye. The inset shows a typical DLS curve for the ME with X_w = 0.42.

We investigate the microenvironment characteristics of the domains in MEs using steady state and time-resolved spectroscopic technique in order to understand the properties of water/oil molecules solubilized into the core. This knowledge is very useful to apply MEs as solubilizing media or as a template in a processes running on the interface between oil and water. The steady state absorption and emission features are presented in Figure 5. In IPM, DCM

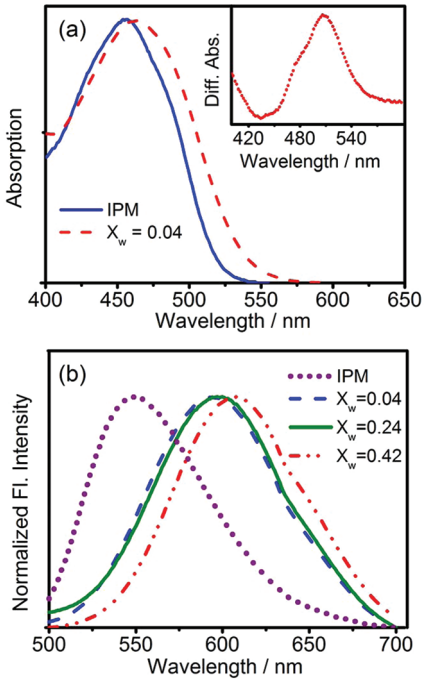

Figure 5. (a) Absorption spectra of DCM in X_w = 0.04 ME and in IPM; the inset shows the difference spectra (in arbitrary units) between DCM in IPM with that of X_w = 0.04 ME. (b) Steady-state emission spectra of DCM excited at 409 nm in IPM and in MEs.

exhibits an absorption peak at 455 nm (Figure 5a). But in MEs with X_w = 0.04, the absorption peak is red-shifted to 465 nm (Figure 5a). The difference of the absorption spectra of DCM in MEs with that of DCM in IPM exhibits a negative absorption or depletion at 455 nm and a distinct peak at 510 nm (Figure 5a, inset). The negative absorption at 455 nm clearly indicates that upon addition of surfactants and water, the population of DCM in the bulk IPM decreases. On the other hand, the emergence of the positive absorption peak at 510 nm indicates that in the presence of surfactants and water, the DCM molecules migrate to a highly polar region, which is presumably due to the influence of the ME. The fluorescence spectra of DCM strongly depends on the polarity of the medium[43] and hence could act as a good reporter for the microenvironment of ME. Figure 5b is a representative illustration of the steady state emission spectra of DCM at various X_w values excited at 409 nm. The corresponding emission peaks (λ_{max}) are presented in Table 1. As is evidenced from the table, the emission peaks are

Table 1. Steady State Fluorescence Peak (λ_{max}), Fittings Parameters of the Solvent Correlation Function ($C(t)$) for the Probe DCM in MEs of Various X_w Values[a]

wt. fraction of water (X_w)	fluorescence peak, λ_{max} (nm)	a_1 (%)	τ_1 (ns)	a_2 (%)	τ_2 (ns)	$\langle\tau_s\rangle$ (ns)	$\Delta\nu$ (cm^{-1})
0.04	596	50	0.15	50	2.06	1.11	1165
0.10	596	56	0.18	44	1.82	0.92	1071
0.20	600	48	0.14	52	1.91	1.06	1060
0.24	600	52	0.17	48	1.62	0.87	1016
0.37	605	56	0.13	44	1.39	0.68	1115
0.42	608	65	0.11	35	0.84	0.37	1073

[a] τ_i represents the solvent correlation time constant, a_i represents its relative contribution and, $\langle\tau_s\rangle$ is the average solvation time constant.

significantly red-shifted compared to DCM in IPM (λ_{max} = 548 nm). It is known that in pure hydrocarbon (e.g., isooctane), the emission peak of DCM is 530 nm, and it is significantly red-shifted to ~620 nm in polar solvent such as methanol.[43] The red-shifted emission peaks in the range of 596−608 nm (Table 1) strongly suggest the presence of a considerable fraction of DCM molecules at the surfactant−water interface of the ME where the microenvironment polarity is expected to be lower compared to that of the water present at the central core of the nanoscopic domain.[44] It could be noted that the emission peak of DCM appears at different wavelengths at different structural domains of the ME (Table 1). This observation supports our earlier observation regarding the existence of different structural entities at various X_w values and reveals the different micropolarity experienced by the probe at respective aggregates. The minor red shift of the emission peak on going from X_w = 0.37 to 0.42 for o/w ME is notable and is discussed later.

The probe DCM has previously been used to report the solvation dynamics of various organized nano assemblies.[45,46] Here, we study the solvation dynamics of the probe in the ME system and investigate in detail the effect of confinement on water relaxation dynamics with different structures of identical composing elements. Figure 6a and Figure S3 (Supporting Information)show the decay transients of DCM at three selected wavelengths of 540 (at the blue end of the spectrum), 600 (around the peak position), and 670 (at the red end of the spectrum) nm for ME of different hydration levels (X_w). It is evidenced from the figures that the decay pattern is strongly wavelength dependent for all the systems studied. For example, at X_w = 0.04 (Figure 6a) the blue end (540 nm) decays with the fitted four-exponential time constants of 0.07 ns (62%), 0.35 ns (22%), 1.19 ns (14%), and 3.57 ns (2%). The transients get slower with increasing wavelength. For the extreme red wavelength (670 nm), a distinct rise component of 0.07 ns is produced along with the decay components of 1.93 and 4.3 ns.

dx.doi.org/10.1021/la3012124 | Langmuir 2012, 28, 8309−8317

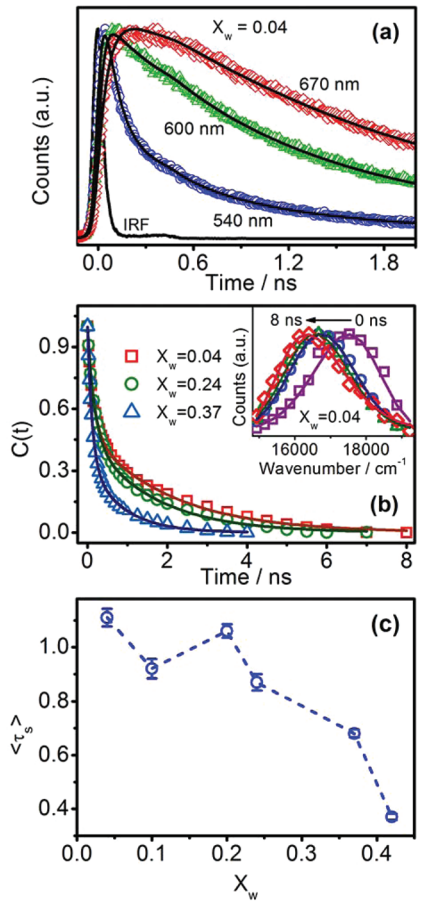

Figure 6. (a) Fluorescence decay transients of DCM in ME with X_w = 0.04. (b) Solvent correlation function, $C(t)$, of DCM in different MEs. The solid lines denote the best fit to biexponential decay. TRES of DCM in ME with X_w = 0.04 are shown in the inset. (c) The average solvation time in ns ($\langle\tau_s\rangle = a_1\tau_1 + a_2\tau_2$) for DCM in MEs of various X_w values. The dotted line is a guide to the eye.

The presence of faster decay components at the blue end and a rise component at the red wavelength is indicative of solvation of the probe in the ME system.

Using the decay transients at different wavelengths, we construct the TRES for different X_w values (inset of Figure 6b and Figure S4). A representative TRES for DCM with X_w = 0.04 is presented in the inset of Figure 6b, wherein a significant dynamic fluorescence Stokes shift of 1165 cm^{-1} in 8 ns is observed. Similar stokes shift for other systems are also listed in Table 1. The solvent correlation function, $C(t)$, obtained for all these systems are fitted with biexponential decay functions based on the core−shell model,[47,48] and the fitted parameters are presented in Table 1. The core−shell model is based on the fact that at least two distinctly different kinds of water molecules are present at the interface of MEs, that is, interfacial (shell) water molecules directly hydrogen bonded to the surfactant headgroups, which displays modified properties compared with bulk water and very slow relaxation dynamics (in the order of nanoseconds), and interior (core) or bulk-like water, which are not directly hydrogen bonded to the surfactant headgroups but have properties slightly different from bulk water.[47,48] Note that both these two types of water molecules relax at a time scale slower than that of bulk water (of the order of sub-picoseconds[49]), which is probably due to the interaction of the surfactant headgroup with water. It is evident from Table 1 that for all the ME structures, one of the solvation time constants is on the order of some hundreds of picoseconds, while the other is on the order of a few nanoseconds. It could be mentioned here that both the observed time constants are orders of magnitude slower than the subpicosecond solvation time constant of bulk water.[49] It is now important to discard any possibility of the observed solvation dynamics by the oil itself since the probe is highly soluble in IPM. Unlike the ME systems, we do not observe any rise component in the decay transient of the IPM/DCM system (data not shown), which clearly indicates the lack of any "slow" solvation present in such system. It has to be mentioned here that a possibility of slow solvation dynamics may arise from the butyl lactate water mixture. We have determined the distribution of butyl lactate between oil phase and water phase and the molar ratio of butyl lactate in oil phase to water is found to be ∼14.3 (Figure S5). To eliminate the possibility of a probable contribution of the butyl lactate/water system toward the observed slow dynamics, we measure the decay transients of a saturated (4.2%, v/v)[17] butyl lactate/water solution. The observed dynamics is rather faster (data not shown) and hardly contribute to the observed slower dynamics of ME systems. The observed slow and relatively fast components for the MEs thus might generate out of the relaxation process by the interfacial bound-type and free-type water molecules, respectively, present in the interface of the ME structure. A similar two-component model consisting of a shell of interfacial water molecules and a bulk-like core has previously been applied to explore the slow dynamics of the water molecules inside various self-assemblies such as micelles,[50] reverse micelles,[51] and lamellar structures.[52] Notably, over the past few years a significant number of studies have been directed toward understanding the water relaxation dynamics in ternary systems with varying parameters such as surfactant charge,[50] effect of counterion,[53] surfactant hydration,[52,54] micellar size,[54−56] morphology of the aggregate,[52,56] and so forth. However, time-resolved solvation dynamics studies led by Levinger et al.[57] show that the solvent reorganization in quaternary micellar systems is significantly slower than in ternary micellar systems, indicating that the probe molecule is located at the micellar interface regardless of alkanol or surfactant. Their study concludes that the environment sensed by the probe C343 in different studied reverse micelles is the same despite the differences in the surfactant or cosurfactant used to make the reverse micelles. Bhattacharyya and co-workers[58] studied the solvation dynamics of 4-aminophthalimide in w/o ME of Triton X-100 in mixed solvents. Their study finds the bimodal solvation response of surrounding water molecules. Despite all these efforts, a detailed systematic investigation of water relaxation dynamics for quaternary MEs of different structural identities with similar composing elements is still lacking and is one of our major concerns in the present study.

Let us compare the solvation dynamics in different nanoassemblies. The slow relaxation dynamics of water as obtained in different structures of ME in the present study have been summarized in Table 1 and Figure 6b. As observed from the table, for w/o ME at low water content (X_w = 0.04), the decay consists of a slow time constant of 2.06 ns and a relatively faster time constant of 0.15 ns. At higher water content (X_w = 0.10), the decay of $C(t)$ is still biexponential, but relatively faster and consists of a component of 1.82 and 0.18 ns with increased contribution of the faster moving bulk water. This observation is justifiable in view of the larger size of the ME for

dx.doi.org/10.1021/la3012124 | Langmuir 2012, 28, 8309−8317

X_w = 0.10 compared to X_w = 0.04 (Figure 4), resulting in an increase in the curvature of the surfactant film, and hence a greater fraction of water interacts with the interface, leading to a relatively faster relaxation.[56,59] In the present study, the time scale obtained for DCM solvation in w/o ME is consistent with that obtained for the same probe in Aerosol-OT (AOT)/*n*-haptane ME with w_0 = 20, where w_0 = [water]/[surfactant].[46] It is to be remembered that the size of AOT reverse ME at w_0 = 20 is comparable[51] to the size range found for the w/o system studied here (Figure 4). In the o/w ME system (X_w = 0.37 and 0.42), it can be observed (Table 1) that the water relaxation dynamics is significantly affected with increasing X_w. The average solvation time ($\langle\tau_s\rangle = a_1\tau_1 + a_2\tau_2$) for X_w = 0.37 is 0.68 ns, whereas it decreases to 0.37 ns for X_w = 0.42. Observing their comparable size (Figure 4), at first, it seems quite contradictory in view of our earlier discussion on water dynamics in a w/o system. However, it should be noted that the λ_{max} value for X_w = 0.42 is red-shifted compared to that of X_w = 0.37 (Table 1), suggesting that in o/w ME with X_w = 0.42, the location of the probe is shifted little toward the bulk water compared to that of X_w = 0.37, and this difference in location is manifested with significantly higher contribution of bulk water with overall faster dynamics of solvation for the latter. At this stage we would like to compare the dynamics of solvation between the two micellar entities just discussed. In many ways, the solvation dynamics of water in o/w ME resembles that of w/o. First, the overall solvation dynamics are significantly slower than those in bulk water[49] and other polar solvents like methanol, acetonitrile, ethylene glycol, and so forth.[60] Second, both of the $C(t)$ functions can be fitted well to biexponential decays. Despite the similarities, the most striking difference is that water dynamics is much faster in the o/w ME compared to w/o (Figure 6c), revealing the confinement of water in the interior of the w/o reverse ME system with restricted translational and rotational motion resulting in a substantially slower dynamics. Now looking into the solvation time components of bicontinuous ME (Table 1), one can similarly see biexponential decay of $C(t)$ with slower relaxation dynamics compared to bulk water. It should be noted here that the structural nature of bicontinuous ME is very complex and quite difficult to predict. The uncertainty lies in its shape, aggregation stability, dimension, and so forth. From Table 1 and Figure 6c, it is evident that with increasing water content, the overall dynamics becomes faster at and beyond $X_w \sim 0.2$, which is quite consistent with the conductivity, viscosity, and sound velocity measurements. The faster solvation time for X_w = 0.24 compared to X_w = 0.20 is believed to be due to the transition of w/o reverse bicontinuous to o/w bicontinuous ME, making the overall dynamics faster with the probe being present in the water continuous region of the latter.

To ascertain the geometrical restriction of the probe in the interfacial region, we measure the time-resolved anisotropy of the probe in selected MEs of different structural identity. Typical anisotropy decays are shown in Figure 7. As observed in Figure 7 and Table 2, all the anisotropy decay transients can be fitted biexponentially. The rotational time constants observed (Table 2) are of the order of hundreds of picoseconds (τ_{fast}) and a few nanoseconds (τ_{slow}), which are in the same order of magnitude as previously reported for micelles[61] with the same probe molecules. The observed τ_{fast} and τ_{slow} could be correlated to the woobling motion and lateral diffusion of the probe molecule, respectively.[62,63] It could be noted that the time components obtained in this study are significantly slower

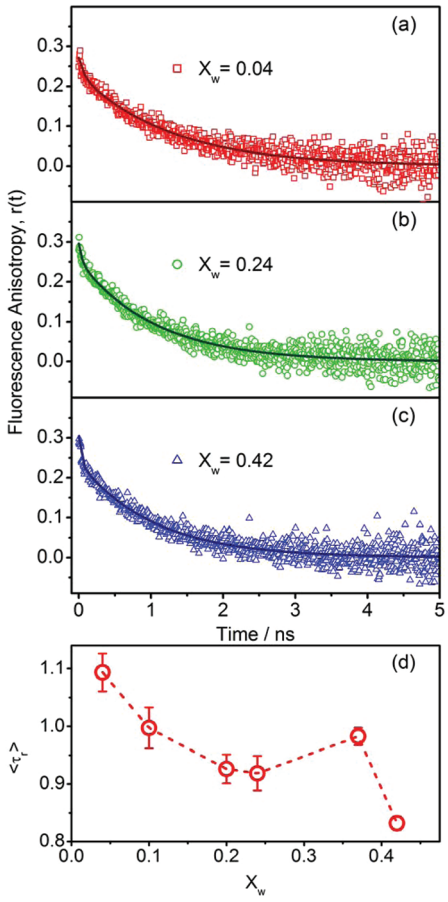

Figure 7. Time-resolved fluorescence anisotropy decay, $r(t)$, of DCM in MEs with (a) X_w = 0.04, (b) X_w = 0.24, and (c) X_w = 0.42. (d) The average rotational anisotropy ($\langle\tau_r\rangle = a_{fast}\tau_{fast} + a_{slow}\tau_{slow}$) values in ns for DCM in MEs of various X_w values. The dotted line is a guide to the eye.

Table 2. Fluorescence Anisotropy Data ($r(t)$) for DCM in MEs at Different X_w Values[a]

wt. fraction of water (X_w)	$r(0)$	a_{fast}	τ_{fast} (ns)	a_{slow}	τ_{slow} (ns)	$\langle\tau_r\rangle$ (ns)
0.04	0.27	0.14	0.07	0.86	1.26	1.09
0.10	0.30	0.24	0.07	0.76	1.29	0.99
0.20	0.26	0.07	0.08	0.93	0.99	0.93
0.24	0.30	0.14	0.05	0.86	1.06	0.92
0.37	0.31	0.25	0.03	0.75	1.30	0.98
0.42	0.30	0.20	0.04	0.80	1.03	0.83

[a] τ_i represents the anisotropy time constant, and a_i represents its relative weight in the total anisotropy.

than the picosecond time scale reported in bulk water,[64] indicating a hindered rotation of the probe in the ME. This shows that the dye experiences higher microviscosity in MEs in comparison to that in bulk water and illustrates the residence of the probe in the interfacial layer of the ME. It could be noted that the $r(0)$ (anisotropy at time zero) values reported in the present systems are smaller than the ideal value of 0.4 (Table 2). The limited resolution of our picoseconds-resolved experimental setup (~ 80 ps IRF) is unable to detect the ultrafast components of the rotational motion, which eventually reduces the $r(0)$ values. We plot the average rotational time constant $\langle\tau_r\rangle$ ($\langle\tau_r\rangle = a_{fast}\tau_{fast} + a_{slow}\tau_{slow}$) against X_w (Figure 7d).

dx.doi.org/10.1021/la3012124 | *Langmuir* 2012, 28, 8309−8317

The figure resembles the solvation profile wherein $\langle\tau_s\rangle$ decreases with increasing X_w. The decreased $\langle\tau_r\rangle$ with increasing X_w indicates progessive release of restriction on the probe, which eventually eases the translational and rotational motion of the probe molecule and hence decreases $\langle\tau_s\rangle$.

CONCLUSION

A novel Tween-based edible ME has been formulated. A large single-phase region is obtained in the pseudoternary phase diagram of the system. The phase behavior of the system remains almost unaltered at low pH (2.6) and in 0.9% salt concentration, which provides a good opportunity for this system to use in drug delivery applications. The pseudoternary system is found to undergo phase transitions from w/o to bicontinuous and from bicontinuous to o/w ME along the water dilution line. The transitions are identified at two distinct X_w values (water weight fraction) using conductivity, viscosity, ultrasonic compressibility, and velocity studies. Micropolarity of the ME environments are successfully probed by the solvatochromic dye DCM. Both steady-state absorption and emission spectra show the dye to reside in the surfactant water interface of the MEs and suggest the efficacy of the MEs to host the model drug/ligand DCM. The significant rotational hindrance of the dye in time-resolved fluorescence anisotropy study further confirms its presence at the interface. The dynamical solvation of water in the ME has been unveiled using picoseconds time-resolved fluorescence spectroscopy. The study finds strong correlation in the relaxation dynamics of water with the structure of host assembly and offers an edible ME system which could act as a potential drug delivery system and nontoxic nanotemplate for other applications.

ASSOCIATED CONTENT

Supporting Information

Pseudoternary phase diagram of a Tween/*n*-butanol/IPM/water ME system at pH 2.6 and normal water, fluorescence decay transients of DCM in MEs of different X_w values, TRES of DCM in MEs of various X_w values, and standard curve for the butyl lactate distribution in oil and water. This material is available free of charge via the Internet at http://pubs.acs.org.

AUTHOR INFORMATION

Corresponding Author

*E-mail: rajib@bose.res.in (R.K.M.); skpal@bose.res.in (S.K.P.). Telephone: +91 033 2335 5706-08. Fax: +91 033 2335 3477.

Notes

The authors declare no competing financial interest.

ACKNOWLEDGMENTS

S.R. thanks CSIR for fellowship. We thank DST for financial support (SR/SO/BB-15/2007).

REFERENCES

(1) Mehta, S. K.; Kaur, G.; Bhasin, K. K. Analysis of Tween Based Microemulsion in the Presence of TB Drug Rifampicin. *Colloids Surf., B* **2007**, *60*, 95−04.

(2) Sintov, A. C.; Shapiro, L. New Microemulsion Vehicle Facilitates Percutaneous Penetration in Vitro and Cutaneous Drug Bioavailability in Vivo. *J. Controlled Release* **2004**, *95*, 173−183.

(3) Venable, R. L.; Elders, K. L.; Fang, J. Microemulsions with High Water Solubilizing Capacity at High Hydrocarbon Levels and Very Low Surfactant Concentrations. *J. Colloid Interface Sci.* **1986**, *109*, 330−335.

(4) Trotta, M.; Gasco, M. R.; Morel, S. Release of Drugs from Oil−Water Microemulsions. *J. Controlled Release* **1989**, *10*, 237−243.

(5) Rosano, H. L.; Cavallo, J. L.; Chang, D. L.; Whittam, J. H. Microemulsions, A Commentary on Their Preparation. *J. Soc. Cosmet. Chem.* **1988**, *39*, 201−209.

(6) Moreira, L. A.; Firoozabadi, A. Thermodynamic Modeling of the Duality of Linear 1-Alcohols as Cosurfactants and Cosolvents in Self-Assembly of Surfactant Molecules. *Langmuir* **2009**, *25*, 12101−12113.

(7) Blank, I. H. Action of Soap on the Skin. *Arch. Dermatol.* **1939**, *39*, 811−817.

(8) Effendy, I.; Maibach, H. I. Surfactants and Experimental Irritant Contact Dermatitis. *Contact Derm* **1995**, *33*, 217−225.

(9) Kogan, A.; Garti, N. Microemulsions as Transdermal Drug Delivery Vehicles. *Adv. Colloid Interface Sci.* **2006**, *123−126*, 369−385.

(10) Venable, R. L.; Viox, D. H. A Microemulsion Cosurfactant with Excellent Water Solubilization at High Oil Content. *J. Dispersion Sci. Technol.* **1984**, *5*, 73−80.

(11) Sagitani, H.; Friberg, S. E. Microemulsion Systems with a Nonionic Cosurfactant. *J. Dispersion Sci. Technol.* **1980**, *1*, 151−164.

(12) Chew, C. H.; Gan, L. M.; Koh, L. L.; Wong, M. K. Microemulsion Systems with Monobutyl Ether of Ethylene Glycol or Diethylene Glycol as Cosurfactant. *J. Dispersion Sci. Technol.* **1988**, *9*, 17−31.

(13) Rowe, R. C.; Sheskey, P. J.; Owen, S. C. *Handbook of Pharmaceutical Excipients*;, 5th ed.; Pharmaceutical Press and American Pharmacists Association: London, 2006.

(14) Comelles, F.; Pascual, A. Microemulsions with Butyl Lactate as Cosurfactant. *J. Dispersion Sci. Technol.* **1997**, *18*, 161−175.

(15) Lactic acid, ethyl ester and Lactic acid, *n*-butyl ester; Exemptions from the Requirement of a Tolerance, by U.S. Enviornmental Protection Agency, Federal Register: 3rd September, 2002, Volume *67*, Number 170, pp 56225−56229, https://www.federalregister.gov/articles/2002/09/03/02-22369/lactic-acid-ethyl-ester-and-lactic-acid-n-butyl-ester-exemptions-from-the-requirement-of-a-tolerance#p-24.

(16) FDA part 172-food additives permitted for direct addition to food for human consumption, Code of Federal Regulations, 2011, Title 21, Volume 3, http://www.accessdata.fda.gov/scripts/cdrh/cfdocs/cfcfr/CFRSearch.cfm?FR=172.515.

(17) Goral, M.; Shaw, D. G.; Maczynski, A.; Wisniewska-Goclowska, B. IUPAC-NIST Solubility Data Series. 88. Esters with Water-Revised and Updated. Part 3. C(7) to C(9) Esters. *J. Phys. Chem. Ref. Data* **2010**, *39*.

(18) Colon, A. A.; Vogel, K. H.; Warner, J. C. The Hydrolysis of Some Alkyl Lactates. II. "Neutral" and Acid Hydrolyses. *J. Am. Chem. Soc.* **1953**, *75*, 6074−6075.

(19) Andersen, F. A. Final Report of the Addendum to the Safety Assessment of *n*-Butyl Alcohol as Used in Cosmetics. *Int. J. Toxicol* **2008**, *27*, 53−69.

(20) Patnaik, P. *A Comprehensive Guide to the Hazardous Properties of Chemical Substances*; John Wiley: New York, 2007.

(21) Reynolds, P. A.; Gilbert, E. P.; White, J. W. High Internal Phase Water-in-Oil Emulsions and Related Microemulsions Studied by Small Angle Neutron Scattering. 2. The Distribution of Surfactant. *J. Phys. Chem. B* **2001**, *105*, 6925−6932.

(22) Benjamins, J.-W.; Thuresson, K.; Nylander, T. Formation of a Liquid Crystalline Phase from Phosphatidylcholine at the Oil−Aqueous Interface. *Langmuir* **2005**, *21*, 2804−2810.

(23) Söderman, O.; Nydén, M. NMR in Microemulsions. NMR Translational Diffusion Studies of a Model Microemulsion. *Colloids Surf., A* **1999**, *158*, 273−280.

(24) Giustini, M.; Palazzo, G.; Colafemmina, G.; Monica, M. D.; Giomini, M.; Ceglie, A. Microstructure and Dynamics of the Water-in-Oil CTAB/*n*-Pentanol/*n*-Hexane/Water Microemulsion: A Spectroscopic and Conductivity Study. *J. Phys. Chem.* **1996**, *100*, 3190−3198.

(25) Nandi, N.; Bhattacharyya, K.; Bagchi, B. Dielectric Relaxation and Solvation Dynamics of Water in Complex Chemical and Biological Systems. *Chem. Rev.* **2000**, *100*, 2013−2045.

(26) Maestro, M. Enzymatic Activity in Reverse Micelles-some Modellistic Considerations on Bell-Shaped Curves. *J. Mol. Liq.* **1989**, *42*, 71−82.
(27) Garti, N.; Aserin, A.; Tiunova, I.; Ezrahi, S. Sub-zero Temperature Behavior of Water in Non-ionic Microemulsions. *J. Therm. Anal. Calorim.* **1998**, *51*, 63−78.
(28) Amararene, A.; Gindre, M.; Huérou, J.-Y. L.; Nicot, C.; Urbach, W.; Waks, M. Water Confined in Reverse Micelles: Acoustic and Densimetric Studies. *J. Phys. Chem. B* **1997**, *101*, 10751−10756.
(29) Isopropyl Myristate; Tolerance Exemption. http://www.epa.gov/fedrgstr/EPA-PEST/1995/February/Day-01/pr-126.html
(30) Campo, L. d.; Yaghmur, A.; Garti, N.; Leser, M. E.; Folmer, B.; Glatter, O. Five-Component Food-Grade Microemulsions: Structural Characterization by SANS. *J. Colloid Interface Sci.* **2004**, *274*, 251−267.
(31) Lakowicz, J. R. *Principles of Fluorescence Spectroscopy*; Kluwer Academic/Plenum: New York, 1999.
(32) Horng, M. L.; Gardecki, J. A.; Papazyan, A.; Maroncelli, M. Subpicosecond Measurements of Polar Solvation Dynamics: Coumarin 153 Revisited. *J. Phys. Chem.* **1995**, *99*, 17311−17337.
(33) Ezrahi, S.; Wachtel, E.; Aserin, A.; Garti, N. Structural Polymorphism in a Four-Component Nonionic Microemulsion. *J. Colloid Interface Sci.* **1997**, *191*, 277−290.
(34) Billman, J. F.; Kaler, E. W. Structure and Phase Behavior in Four-Component Nonionic Microemulsions. *Langmuir* **1991**, *7*, 1609−1617.
(35) Arvidsson, A.; Söderman, O. The Microemulsion Phase in the Didecyldimethylammonium Bromide/Dodecane/Water System. Phase Diagram, Microstructure, and Nucleation Kinetics of Excess Oil Phase. *Langmuir* **2001**, *17*, 3567−3572.
(36) Podlogar, F.; Rogač, M. B.; Gašperlin, M. The Effect of Internal Structure of Selected Water−Tween 40®−Imwitor 308®−IPM Microemulsions on Ketoprofene Release. *Int. J. Pharm.* **2005**, *302*, 68−77.
(37) Yaghmur, A.; Aserin, A.; Antalek, B.; Garti, N. Microstructure Considerations of New Five-Component Winsor IV Food-Grade Microemulsions Studied by Pulsed Gradient Spin−Echo NMR, Conductivity, and Viscosity. *Langmuir* **2003**, *19*, 1063−1068.
(38) Mitra, R. K.; Paul, B. K. Physicochemical Investigations of Microemulsification of Eucalyptus Oil and Water Using Mixed Surfactants (AOT + Brij-35) and Butanol. *J. Colloid Interface Sci.* **2005**, *283*, 565−577.
(39) Gradzielski, M.; Hoffman, H. Rheological Properties of Microemulsions. In *Handbook of Microemulsion Science and Technology*, Kumar, P.; Mittal, K. L., Eds.; Marcel Dekker: New York, 1999; pp 161−192.
(40) Saidi, Z.; Mathew, C.; Peyrelasse, J.; Boned, C. Percolation and Critical Exponents for the Viscosity of Microemulsions. *Phys. Rev. A* **1990**, *42*, 872−876.
(41) Rojas, O.; Koetz, J.; Kosmella, S.; Tiersch, B.; Wacker, P.; Kramer, M. Structural Studies of Ionic Liquid-Modified Microemulsions. *J. Colloid Interface Sci.* **2009**, *333*, 782−790.
(42) Polizelli, M. A.; Telis, V. R. N.; Amaral, L. Q.; Feitosa, E. Formation and Characterization of Soy Bean Oil/Surfactant/Water Microemulsions. *Colloids Surf., A* **2006**, *281*, 230−236.
(43) Meyer, M.; Mialocq, J. C. Ground State and Singlet Excited State of Laser Dye DCM: Dipole Moments and Solvent Induced Spectral Shifts. *Opt. Commun.* **1987**, *64*, 264−268.
(44) Geddes, C. D.; Lakowicz, J. R. *Reviews in Fluorescence*; Springer: New York, 2005.
(45) Saha, R.; Verma, P. K.; Mitra, R. K.; Pal, S. K. Structural and Dynamical Characterization of Unilamellar AOT Vesicles in Aqueous Solutions and Their Efficacy as Potential Drug Delivery Vehicle. *Colloids Surf., B* **2011**, *88*, 345−353.
(46) Pal, S. K.; Mandal, D.; Sukul, D.; Bhattacharyya, K. Solvation Dynamics of 4-(dicyanomethylene)-2-methyl-6-(p-dimethylaminostyryl)-4H-pyran (DCM) in a Microemulsion. *Chem. Phys. Lett.* **1999**, *312*, 178−184.
(47) Piletic, I. R.; Moilanen, D. E.; Spry, D. B.; Levinger, N. E.; Fayer, M. D. Testing the Core/Shell Model of Nanoconfined Water in Reverse Micelles Using Linear and Nonlinear IR Spectroscopy. *J. Phys. Chem. A* **2006**, *110*, 4985−4999.
(48) Faeder, J.; Ladanyi, B. M. Molecular Dynamics Simulations of the Interior of Aqueous Reverse Micelles. *J. Phys. Chem. B* **2000**, *104*, 1033−1046.
(49) Jimenez, R.; Fleming, G. R.; Kumar, P. V.; Maroncelli, M. Femtosecond Solvation Dynamics of Water. *Nature* **1994**, *369*, 471−473.
(50) Tamoto, Y.; Segawa, H.; Shirota, H. Solvation Dynamics in Aqueous Anionic and Cationic Micelle Solutions: Sodium Alkyl Sulfate and Akyltrimethylammonium Bromide. *Langmuir* **2005**, *21*, 3757−3764.
(51) Mitra, R. K.; Sinha, S. S.; Pal, S. K. Temperature-Dependent Solvation Dynamics of Water in AOT/Isooctane Reverse Micelles. *Langmuir* **2008**, *24*, 49−56.
(52) Verma, P. K.; Saha, R.; Mitra, R. K.; Pal, S. K. Slow Water Dynamics at the Surface of Macromolecular Assemblies of Different Morphologies. *Soft Matter* **2010**, *6*, 5971−5979.
(53) Harpham, M. R.; Ladanyi, B. M.; Levinger, N. E. The Effect of the Counterion on Water Mobility in Reverse Micelles Studied by Molecular Dynamics Simulations. *J. Phys. Chem. B* **2005**, *109*, 16891−16900.
(54) Kumbhakar, M.; Nath, S.; Mukherjee, T.; Pal, H. Solvation Dynamics in Triton-X-100 and Triton-X-165 Micelles: Effect of Micellar Size and Hydration. *J. Chem. Phys.* **2004**, *121*, 6026−6033.
(55) Willard, D. M.; Riter, R. E.; Levinger, N. E. Dynamics of Polar Solvation in Lecithin/Water/Cyclohexane Reverse Micelles. *J. Am. Chem. Soc.* **1998**, *120*, 4151−4160.
(56) Willard, D. M.; Levinger, N. E. Influence of Morphology on Polar Solvation Dynamics in Lecithin Reverse Micelles. *J. Phys. Chem. B.* **2000**, *104*, 11075−11080.
(57) Corbeil, E. M.; Levinger, N. E. Dynamics of Polar Solvation in Quaternary Microemulsions. *Langmuir* **2003**, *19*, 7264−7270.
(58) Mandal, D.; Datta, A.; Pal, S. K.; Bhattacharyya, K. Solvation Dynamics of 4-Aminophthalimide in Water-in-Oil Microemulsion of Triton X-100 in Mixed Solvents. *J. Phys. Chem. B* **1998**, *102*, 9070−9073.
(59) Moilanen, D. E.; Fenn, E. E.; Wong, D.; Fayer, M. D. Water Dynamics in Large and Small Reverse Micelles: From Two Ensembles to Collective Behavior. *J. Chem. Phys.* **2009**, *131*, 014704−014712.
(60) Meulen, P. v. d.; Zhang, H.; Jonkman, A. M.; Glasbeek, M. Subpicosecond Solvation Relaxation of 4-(Dicyanomethylene)-2-methyl-6-(p-(dimethylamino)styryl)-4H-pyran in Polar Liquids. *J. Phys. Chem.* **1996**, *100*, 5367−5373.
(61) Mitra, R. K.; Sinha, S. S.; Pal, S. K. Temperature Dependent Hydration at Micellar Surface: Activation Energy Barrier Crossing Model Revisited. *J. Phys. Chem. B* **2007**, *111*, 7577−7583.
(62) Lipari, G.; Szabo, A. Model-Free Approach to the Interpretation of Nuclear Magnetic Resonance Relaxation in Macromolecules. 1. Theory and Range of Validity. *J. Am. Chem. Soc.* **1982**, *104*, 4546−4559.
(63) Wang, C. C.; Pecora, R. Time-Correlation Functions for Restricted Rotational Diffusion. *J. Chem. Phys.* **1980**, *72*, 5333−5340.
(64) Banerjee, D.; Verma, P. K.; Pal, S. K. Temperature-Dependent Femtosecond-Resolved Hydration Dynamics of Water in Aqueous Guanidinium Hydrochloride Solution. *Photochem. Photobiol. Sci.* **2009**, *8*, 1441−1447.